RSC Advances

PAPER

View Article Online
View Journal | View Issue

Cite this: *RSC Adv.*, 2021, **11**, 31783

A biomimetic orthogonal-bilayer tubular scaffold for the co-culture of endothelial cells and smooth muscle cells

Mei-Xi Li,[ab] Lei Li, *[ac] Si-Yuan Zhou,[ab] Jian-Hua Cao,[a] Wei-Hua Liang,[a] Ye Tian, [ad] Xue-Tao Shi, [e] Xiu-Bin Yang[f] and Da-Yong Wu *[a]

Received 9th June 2021
Accepted 17th September 2021

DOI: 10.1039/d1ra04472a

rsc.li/rsc-advances

In blood vessels, endothelial cells (ECs) grow along the direction of blood flow, while smooth muscle cells (SMCs) grow circumferentially along the vessel wall. To mimic this structure, a polycaprolactone (PCL) tubular scaffold with orthogonally oriented bilayer nanofibers was prepared *via* electrospinning and winding. ECs were cultured on the inner layer of the scaffold with axial nanofibers and SMCs were cultured on the outer layer of the scaffold with circumferential nanofibers. Fluorescence images of the F-actin distribution of ECs and SMCs indicated that cells adhered, stretched, and proliferated in an oriented manner on the scaffold. Moreover, layers of ECs and SMCs formed on the scaffold after one month of incubation. The expression levels of platelet-endothelial cell adhesion molecule 1 (PECAM-1) and a contractile SMC phenotype marker in the EC/SMC co-culture system were much higher than those in individual culture systems, thus demonstrating that the proposed biomimetic scaffold promoted the intercellular junction of ECs and preserved the contractile phenotype of SMCs.

1. Introduction

Cardiovascular disease has become a leading cause of morbidity and mortality worldwide.[1,2] In clinical applications, vascular grafts play an important role in the treatment of cardiovascular diseases.[3,4] Nevertheless, natural sources of autogenous blood vessels are too limited to meet therapeutic needs,[5,6] and therefore artificial vascular grafts are often used to repair damaged and obstructed blood vessels. Satisfactory results have been achieved using large- and medium-diameter vascular grafts. However, the long-term patency rates of small-diameter vascular grafts (inner diameter < 6 mm) remain problematic.[7]

The development of *in vitro* models that mimic the key anatomical and physiological features of blood vessels would help to understand the mechanism of maintaining vascular patency and improve the design of vascular grafts. The innermost tunica of a blood vessel is made up of one layer of endothelial cells (ECs), which align and elongate in the direction of fluid flow. Surrounding the tunica intima is the tunica media, which mainly consists of circumferentially arranged smooth muscle cells (SMCs). Various types of EC/SMC co-culture systems have been proposed.[8–10] However, given that the alignment of ECs and SMCs is orthogonal, co-culture of ECs and SMCs with their respective cellular configurations on a tubular scaffold remains an important challenge.

In recent years, several EC/SMC co-culture systems have been developed to mimic blood vessel structures and native vascular cell alignment. For example, in a biomimetic *in vivo*-like vasculature, a microwrinkle pattern was used to lead a circumferential SMC layer and the shear stress was applied to induce ECs to orient parallel to the axis.[11] It takes several steps to obtain the circular microfluidic channel with circumferential microwrinkle patterns. Another study employed a triple coaxial nozzle to form a bilayer tubular structure encapsulating ECs and SMCs in their respective layers and applied shear stress during the extrusion process to orientate the cells in the desired directions.[12] Both methods require the continuous use of syringe pumps to provide shear stress, which increases the complexity of the system. Moreover, it is difficult to induce ECs and SMCs growing on the tubular scaffold in orthogonal directions only by shear forces, since shear force acts parallel to the surface boundary of the cells and induces cells growth in the direction of the shear force.[13,14] Therefore, a simple method for the fabrication of tubular scaffolds with the representative structure

[a]*Technical Institute of Physics and Chemistry, Chinese Academy of Sciences, Beijing 100190, P. R. China. E-mail: dayongwu@mail.ipc.ac.cn; lileilei@mail.ipc.ac.cn*
[b]*University of Chinese Academy of Sciences, Beijing 100049, P. R. China*
[c]*CAS Key Laboratory of Cryogenics, Technical Institute of Physics and Chemistry, Chinese Academy of Sciences, Beijing 100190, P. R. China*
[d]*Key Laboratory of Photochemical Conversion and Optoelectronic Materials, Technical Institute of Physics and Chemistry, Chinese Academy of Sciences, Beijing 100190, P. R. China*
[e]*National Engineering Research Center for Tissue Restoration and Reconstruction, South China University of Technology, Guangzhou 510006, P. R. China*
[f]*Department of Cardiac Surgery, Beijing Institute of Heart, Lung and Blood Vessel Diseases, Beijing Anzhen Hospital, Capital Medical University, Beijing 100029, P. R. China*

of the tunica intima and tunica media *via* the orthogonal co-culture of ECs and SMCs is still expected.

In addition to surface patterns and shear stress, the aligned fibers produced by electrospinning could also guide cell growth and orientation.[15,16] Electrospinning is a cost-effective and promising approach for the preparation of nanofibers at room temperature and has therefore been widely applied in the field of tissue engineering.[17–19] Electrospun fibers containing natural aloe vera skin extract (AVE) can be used as antioxidant wound dressings.[20] The fibers have a similar morphological structure to that of the native extracellular matrix and are suitable to entrap active compounds and control substance release.[21,22] Further, the high specific surface area of the fibers promotes cell adhesion and proliferation, whereas its high porosity can provide more growth space for cells and facilitate intercellular communication. Additionally, compared with randomly oriented fibers, aligned fibers exhibit enhanced matrix deposition and increased tensile properties along the fiber direction.[23,24] Electrospun fibers with controllable sizes ranging from nanometers to micrometers can effectively induce cell orientation without the need for additional devices. Therefore, inducing the growth of ECs and SMCs by combining two layers of nanofibers with different orientations can be a practical and promising approach. Polycaprolactone (PCL) is a Food and Drug Administration (FDA)-approved material and has been widely used in clinic applications for many implant-based products.[25] This material was thus selected for the fabrication of the tubular scaffold due to its malleability, biocompatibility, biodegradability, and low price.[26,27]

To the best of our knowledge, this is the first time that ECs and SMCs grew in orthogonal directions on a tubular scaffold induced only by aligned fibers. Compared with shear force induction, our approach can effectively induce cell orientation without additional auxiliary device. Moreover, ECs and SMCs were cultured on the inner and outer layers of the tubular scaffold, respectively, and were successfully oriented in the desired directions. The axial fibers of the inner layer and circumferential fibers of the outer layer of the tubular scaffold were orthogonally oriented, thus facilitating the induction of EC and outer SMC growth in orthogonal directions. The orthogonal-bilayer tubular scaffold could promote the connection of ECs and the preservation of the contractile phenotype of SMCs. Therefore, the proposed biomimetic orthogonal-bilayer tubular scaffold could provide important insights into the design of artificial vascular grafts.

The morphology of the scaffold was observed *via* field emission scanning electron microscopy (FE-SEM). Tensile properties were assessed using a universal testing machine (INSTRON 5966). Contact angles were measured using a video-based contact angle measuring device (OCA-20). Functional groups on the surface of the scaffold were detected and characterized *via* Fourier transform infrared spectrometry (FTIR). Cell morphology was characterized *via* fluorescence staining and SEM. The expression of cluster of differentiation 31 (CD31) was observed *via* an immunofluorescence assay. The gene expression levels of α-smooth muscle actin (α-SMA) and osteopontin (OPN) of SMCs were measured *via* quantitative real-time polymerase chain reaction (qRT-PCR).

2. Materials and methods

2.1. Materials

Polycaprolactone (PCL, M_n 80 000), paraformaldehyde (PF, SKU 47608), Triton X-100 (SKU T9284), the mouse anti-CD31 (PECAM-1) antibody (Product no. P8590), and the anti-mouse IgG (whole molecule) TRITC conjugate (Product no. T5393) were purchased from Sigma-Aldrich (St. Louis, MO, USA). Dichloromethane (DCM, Analytical Reagent (AR)) and dimethylacetamide (DMAc, AR) were purchased from Beijing Chemical Works (Beijing, China). ECs, endothelial cell medium (ECM, Cat no. 1001) and fibronectin (FN, Cat no. 8248) were purchased from ScienCell (San Diego, CA, USA). SMCs were obtained from Cell Resource Center (IBMS, CAMS/PUMC). Dulbecco's modified Eagle medium (DMEM, REF 11995-065), fetal bovine serum (FBS, REF 10099-141), penicillin/streptomycin (P/S, REF 15140-122) solution, trypsin (REF 25200-056), and phosphate buffered saline (PBS, REF C 10010500BT) were purchased from Gibco (Grand Island, NY, USA). Alexa Fluor 488 phalloidin (Cat No. A12379), 4′,6-diamidino-2-phenylindole (DAPI, Cat no. D3571), and Trizol reagent (Cat no. 15596-018) were purchased from Invitrogen (Carlsbad, CA, USA).

2.2. Preparation of the orthogonal bilayer tubular scaffold

Fig. 1a illustrates the preparation of the orthogonal bilayer PCL scaffold. First, a PCL film with aligned nanofibers was prepared using a custom-made multifunctional electrospinning machine. The output of the direct current power supply and the receiving distance were set to 15 kV and 15 cm, respectively. PCL was dissolved in DCM/DMAc (9/1, v/v) and stirred for 12 h at room temperature to obtain a 10% w/v solution. At the relative humidity value of approximately 30%, the PCL solution was drawn with a syringe pump at a flow rate of 2.0 mL h^{-1} for 5 h. As the rotation speed increased to 500 rpm, well-aligned PCL fibers were captured using a 20 cm diameter grounded cage collector. The PCL film was then removed from the collector and two pieces were cut and successively rolled onto a 4 mm diameter metal rod. The nanofibers on the inner and outer layers were oriented along the axial and circumferential directions, respectively. Finally, the bilayer PCL films were peeled off from the metal rod to form tubular scaffolds. The scaffolds were then placed in a vacuum oven at room temperature for 12 h to remove the residual solvent.

2.3. Preparation of the heparinized PCL scaffold

To improve the hydrophilicity of the PCL scaffold for cell adhesion, heparin was covalently linked to the scaffold[28,29] as illustrated in Fig. 1b. First, the scaffold reacted with 1,6-hexanediamine in an isopropanol solution (0.43 mol L^{-1}) at 30 °C for 1 h. Then the aminolyzed scaffold was thoroughly rinsed with deionized water three times and dried in a vacuum oven at room temperature. Heparin (1 mg mL^{-1}) was dissolved in 2-(*N*-

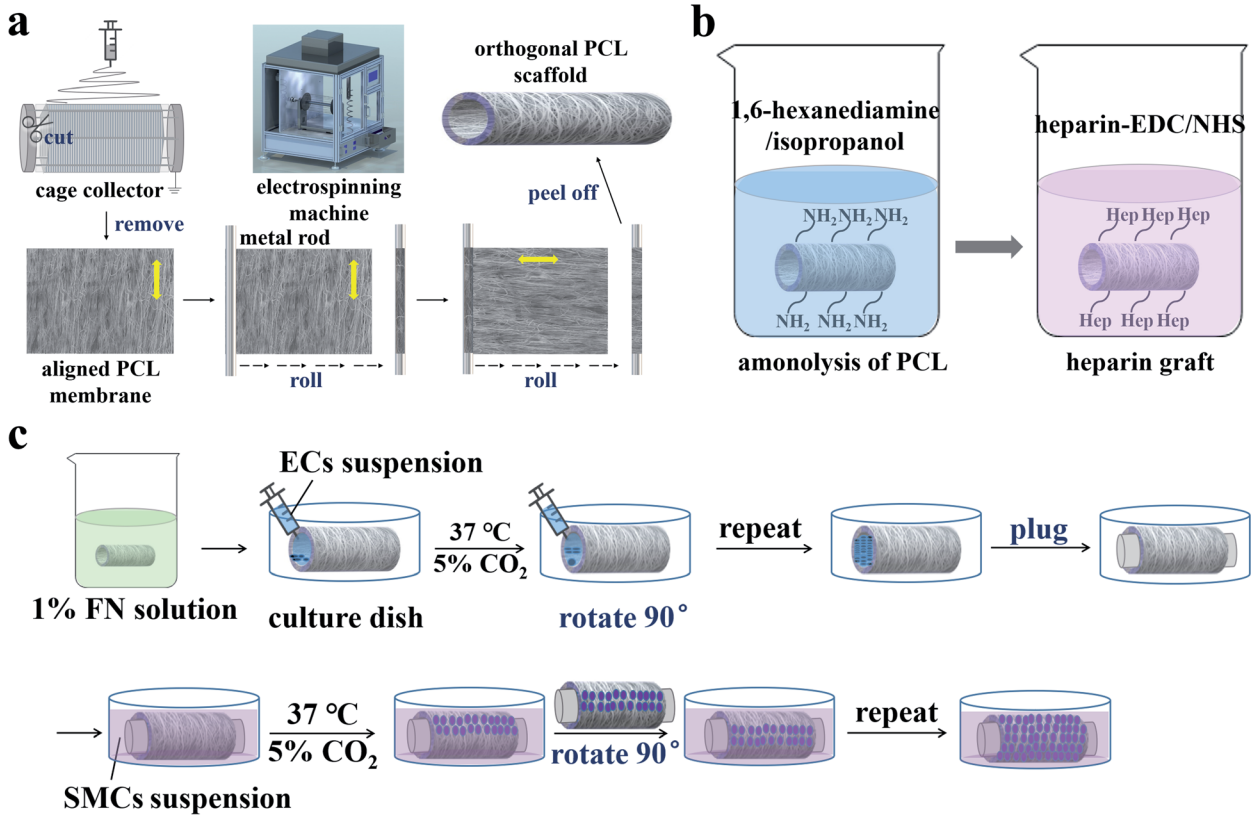

Fig. 1 Schematic diagrams of (a) the orthogonal bilayer PCL scaffold preparation, (b) heparinization, and (c) cell seeding on the scaffold.

morpholine)ethanesulfonic acid (MES) buffer solution (0.10 mol L^{-1}) containing 0.15 mol L^{-1} NHS and 0.30 mol L^{-1} EDC (pH = 5.0), then kept at 30 °C for 4 h. Finally, the aminolyzed scaffold was immersed in active heparin solution at 30 °C for 24 h, then washed three times with deionized water and dried at room temperature.

2.4. Characterization of the PCL tubular scaffold

The surface morphology of the PCL scaffold was observed *via* field emission scanning electron microscopy (FE-SEM, S-4800, Hitachi, Japan) with an accelerating voltage of 10 kV. Before being tested, all samples were sputter-coated with a gold layer using an ion sputtering device (Mc1000, Hitachi, Japan). To assess nanofiber alignment, SEM images were analysed using the ImageJ software. Concretely, 100 fibers were randomly selected from the image to calculate the average orientation angle.

To evaluate the longitudinal tensile properties of the orthogonal bilayer PCL tubular scaffolds, dynamic mechanical analysis measurements were performed in quintuplicate using a universal testing machine (INSTRON 5966, Canton, MA) according to the YY standard 0500-2004/ISO 7198:1998. Both ends of the sample were fixed on two clamps that were set 1 cm apart from each other. A 500 N force was applied and the stretching speed was set to 1 mm min^{-1}. Moreover, to evaluate the hydrophilicity of the scaffolds, contact angels were measured using a video-based contact angle measuring device (OCA-20, DataPhysics Instruments, Germany). At least five 3 μL droplets were used for the measurement. The functional groups on the surface of the scaffold were detected *via* Fourier transform infrared spectrometer (FTIR, Excalibur 3100, Varian, America). 64 scans were performed at a 600–4000 cm^{-1} range with an 8 cm^{-1} resolution.

2.5. Cell culture

ECs were cultured in ECM and SMCs were cultured in complete medium supplemented with 10% FBS and 1% P/S sulphate. The cells were used between 3 to 10 passages. Cells cultured in flasks were treated with trypsin once they reached approximately 80% confluence and then resuspended in medium. Cell densities were adjusted to approximately 5×10^5 cells per mL.

To investigate the guiding effect of the aligned fibers for cell orientation, ECs and SMCs were cultured on the PCL films with aligned and random nanofibers. PCL films were cut into 13 mm-diameter circles. Before cell seeding, the PCL films were heparinized, sterilized, and soaked in 1% FN solution at 4 °C for 12 h, as FN modification reportedly enhances cell–matrix adhesion strength and promotes cell attachment.[30–32]

2.6. Co-culture of ECs and SMCs on the tubular scaffold

Before cell seeding, the tubular scaffolds were heparinized, sterilized, and soaked in 1% FN solution at 4 °C for 12 h. ECs and SMCs were then seeded on the inner and outer layers of the orthogonal tubular scaffold, respectively. The co-culture process is illustrated in Fig. 1c. The tubular scaffold was first placed in the cell culture dish, after which 200 μL of EC suspension (at a density of 5×10^5 cells per mL) was added onto the inner side

of the tubular scaffold. The scaffolds were then placed in a cell incubator at 37 °C and 5% CO_2. After 3 h, the medium was removed from the scaffold, the tubular scaffold was rotated 90°, and the cell suspension was added once more. This step was repeated until the entire inner wall was seeded with ECs. ECM was then added to the tubular scaffold, after which both ends of the tubular scaffold were plugged. Next, the tubular scaffold was immersed in a culture dish with SMC suspension at a 5×10^5 cells per mL density and placed in the incubator. The SMC suspension was changed every 3 h and the tubular scaffold was rotated 90°. This step was repeated until the entire outer wall was seeded with SMCs. The cell culture medium was changed every 24 h, including both the ECM in the tubular scaffold and the SMC medium in the culture dish. Additionally, to investigate the interactions between SMCs and ECs, tubular scaffolds with only ECs cultured on the inner side or only SMCs cultured on the outer side were set as controls.

2.7. Characterization of ECs and SMCs morphology

The morphology of ECs and SMCs cultured on the PCL films (after 2, 4, 6, and 8 days) and the tubular scaffolds (after 10 days) were characterized *via* fluorescence staining and SEM.

2.7.1. Fluorescence staining. The F-actin filaments and nuclei of ECs and SMCs were stained with phalloidin and DAPI solution, respectively. The cells were washed with PBS three times, fixed with 4% PF for 10 min, and then permeabilized with 0.1% Triton X-100 for 15 min. Afterwards, the cells were washed three times with PBS and stained with fluorescent phalloidin conjugate solution (165 nM) in PBS for 20 min at 37 °C. The samples were then rinsed three times with PBS, incubated in DAPI solution (300 nM) for 5 min at 37 °C, and once again rinsed with PBS. An inverted fluorescence microscope (Zeiss, Germany) was used to record fluorescence images and observe cell morphology.

2.7.2. SEM characterization. The samples were washed with PBS, fixed with 2.5% glutaraldehyde solution, and then dehydrated with increasing concentrations of ethanol (50%, 75%, 90%, 95%, and 100%). Before imaging, the samples were sputter-coated with gold for 60 s. Cell morphology was assessed *via* SEM with an accelerating voltage of 10 kV.

2.8. Cluster of differentiation 31 (CD31) immunofluorescence assay

To study the effects of SMCs on ECs function on the co-culture orthogonal-bilayer tubular scaffold, we investigated the expression level of CD31 of ECs. After culturing for 7 days, the scaffolds with ECs cultured on the inner layer (used as control) and with EC/SMC cultured on the inner/outer layers were washed with 4% PF at room temperature for 10 min. After washing, the scaffolds were immersed in 0.1% Triton X-100 for 15 min to enhance cell permeability. Subsequently, the cells were blocked with 5% goat serum in PBS for 1 h and labelled with mouse anti-CD31 at 4 °C for 12 h. After washing with 1% PBS/Tween, the cells were incubated with anti-mouse IgG (whole molecule) TRITC conjugate at 37 °C for 2 h and washed with 1% PBS/Tween. Finally, the cells were stained with DAPI at 37 °C for 5 min. Fluorescence images were observed and recorded *via* confocal microscopy (ARsiMP-LSM-Kit-Legend Elite-USX, Nikon, Japan).

2.9. SMCs gene expression analysis

We also investigated the mRNA expression levels of α-smooth muscle actin (α-SMA) and osteopontin (OPN) of SMCs. After culturing for 1 month, the scaffolds with SMCs cultured on the outer layer (used as control) and with EC/SMC cultured on the inner/outer layers were washed with PBS and immersed in Trizol reagent. α-SMA and OPN expressions were measured *via* quantitative real-time polymerase chain reaction (qRT-PCR). Total RNA was first extracted from the SMCs using the Trizol reagent and converted into cDNA with a reverse transcription kit (Thermo, USA). Afterwards, a SYBR Green kit (Fermentas, Canada) was used to amplify the prepared cDNA. Finally, a real-time detector was used to determine the relative expression of α-SMA and OPN. Glyceraldehyde-3-phosphate dehydrogenase (GAPDH) was used as an endogenous reference. All qRT-PCR primers are listed in Table 1.

2.10. Hematoxylin & eosin (H&E) staining of ECs and SMCs on the tubular scaffold

After 1 month of *in vitro* co-culture, ECs and SMCs on the tubular scaffolds were analysed *via* H&E staining. The scaffold was first washed with PBS and fixed with 4% PF. Then, the scaffold was cut crosswise to obtain a 5 μm thick section using a microtome. Afterwards, H&E staining was performed using an automatic stainer (Micron HMS 740, Thermo Scientific, Germany) according to standard histological procedures. Finally, the section was mounted for observation under a laser scanning quantitative imaging system (VECTRA, PerkinElmer, USA).

3. Results and discussion

3.1. Characterization of the orthogonal-bilayer tubular scaffold

Fig. 2a shows a photograph of the scaffold. The outer diameter and the wall thickness of the scaffold were 4 ± 0.02 mm and 135 ± 1.11 μm, respectively. SEM imaging (Fig. 2b) showed that the

Table 1 Primer sequences used in the experiments

genes	Primer F (5′–3′)	Primer R (5′–3′)
α-SMA	CGAAGCACAGAGCAAAAGAGG	TCAGGGGCAACACGAAGC
OPN	CAGTGATTTGCTTTTGCCTCC	TGGCTTTCGTTGGACTTACTTG
GAPDH	AATCCCATCACCATCTTC	AGGCTGTTGTCATACTTC

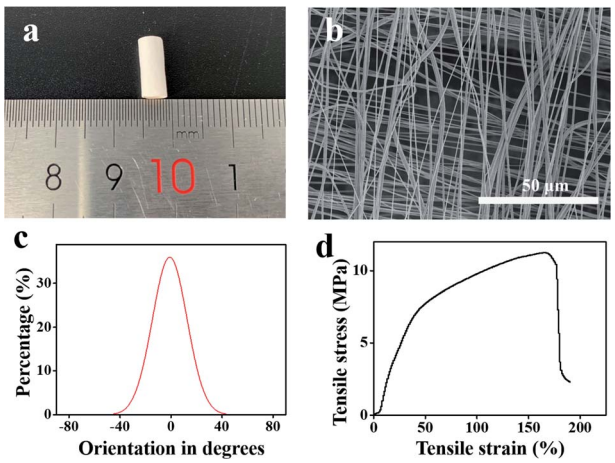

Fig. 2 (a) A picture of the PCL tubular scaffold. (b) SEM image of the PCL tubular scaffold. (c) Distribution of the orientation angles between the long axes of the nanofibers and their expected directions. (d) Mechanical properties of the orthogonal-bilayer PCL tubular scaffold.

scaffold was composed of two layers and the fiber direction of these two layers was orthogonal. The diameter of the nanofibers was 664 ± 163 nm. The orientation angle distribution curve of the nanofibers was calculated using the ImageJ software (Fig. 2c). The full width at half maximum (FWHM) of the distribution curve was 24°, indicating that each layer exhibited a good orientation. The mechanical properties of the orthogonal-bilayer tubular scaffold were also measured, and the stress–strain curve is illustrated in Fig. 2d. Young's modulus was 30.69 ± 2.92 MPa, which was calculated with the Bluebill software. The tensile stress was 10.34 ± 1.14 MPa, which was similar to that of the native human coronary arteries (1.40–11.14 MPa).[33] The ultimate strain was 191.2 ± 11.9%, which was higher than that of the native human coronary arteries (45–99%).[33]

3.2. Characterization of the heparinized PCL scaffold

The surface properties of the scaffold significantly affect the adhesion between the substrate and cells. Heparin is a natural anticoagulant that is often employed to modify the surfaces of vascular scaffolds to make them hydrophilic and favour cell adhesion.[34–36] Therefore, heparin was grafted onto the scaffold, after which FTIR was used to characterize the absorption peaks. As shown in Fig. 3a, the characteristic absorption peaks of PCL were 1730 cm^{-1} (C=O stretching vibration) and 1170 cm^{-1} (C–O–C stretching vibration),[28] and those of heparin were approximately 3000–3700 cm^{-1} (amine stretching vibrations) and 1620 cm^{-1} (protonated amine vibration).[28,37] Clear absorption peaks were observed at 3290 cm^{-1}, 1730 cm^{-1}, 1620 cm^{-1}, and 1170 cm^{-1} in the heparinized PCL spectrum.[38] The peak intensity at approximately 3290 cm^{-1} was weaker than that of the heparin spectrum, indicating a decrease in the free hydroxyl groups on the carboxyl moiety of heparin and confirming that heparin was successfully grafted onto the PCL surface. The contact angles of water on the scaffold surfaces were also measured. Heparin contains abundant polar groups, such as sulfuric acid groups and carboxyl, which improve the hydrophilicity of the scaffold.[39] Our results indicated that the contact angles were 130.7 ± 1.0° (hydrophobic) and 35.9 ± 0.7° (hydrophilic) before and after heparin grafting, respectively (Fig. 3b and c), which indicated that heparinization can significantly improve the hydrophilicity of the scaffold.

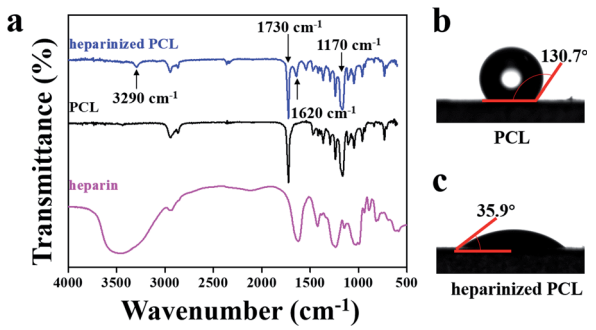

Fig. 3 (a) FTIR spectra of PCL, heparinized PCL and heparin. (b) Contact angle of water on PCL. (c) Contact angle of water on heparinized PCL.

3.3. Cell culture on the heparinized PCL film

We first demonstrated that ECs and SMCs could adhere and proliferate on the heparinized PCL film and that the PCL film with aligned fibers could induce cell orientation. ECs and SMCs were seeded onto the heparinized PCL films with random and aligned fibers. After 2, 4, 6, and 8 days of incubation, the F-actin and nuclei of the cells were stained (Fig. 4a). Both ECs and SMCs grew well on the heparinized PCL films and the cells were aligned along the fiber orientation direction on the film with aligned fibers. SEM images (Fig. 4b) also showed that both ECs and SMCs could adhere and align well on the aligned fibers. The

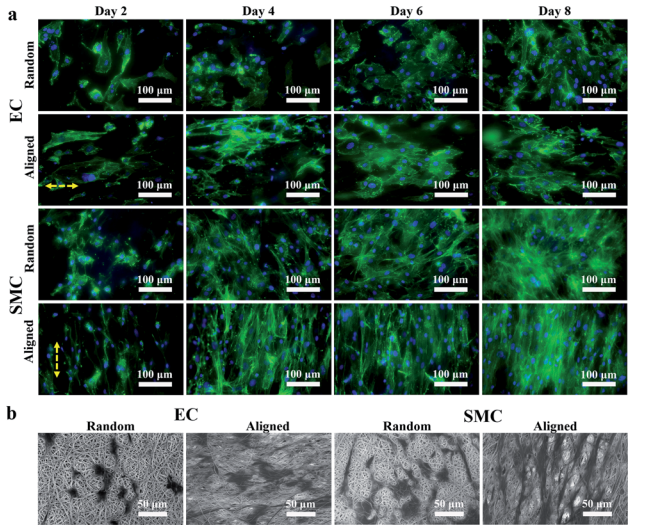

Fig. 4 (a) Fluorescence images of ECs and SMCs seeded on the heparinized PCL film with random and aligned fibers. After 2, 4, 6, and 8 days of incubation, the cells were stained with phalloidin (green) and DAPI (blue). (b) SEM images of ECs and SMCs on the aligned and random PCL films after 2 days of incubation.

Table 2 The angle between the spread of the cytoskeleton and horizontal direction

Orientation	Angle (°)
EC (random)	50.5 ± 16.0
EC (aligned)	19.0 ± 8.6
SMC (random)	84.4 ± 45.9
SMC (aligned)	82.0 ± 4.4

angle between the spread of the cytoskeleton and the horizontal direction of ECs and SMCs cultured for 8 days on the random and aligned fibers was calculated using ImageJ software (Table 2). We randomly selected 100 cytoskeletons for calculation. It was shown that the standard deviation of the angle between the spread of the cytoskeleton and horizontal direction was evidently smaller on the aligned fibers than that on the random fibers, which indicated that aligned fibers can effectively induce cell orientation.

3.4. Orthogonal co-culture of ECs and SMCs on the tubular scaffold

After proving that the PCL film with aligned fibers could induce the orientation of ECs and SMCs, we investigated the co-culture of ECs and SMCs on the orthogonal bilayer tubular scaffold. Fluorescent staining images and SEM images of ECs on the inner layer and SMCs on the outer layer after 10 days of co-culture are shown in Fig. 5a. As shown in Fig. 5a, ECs and SMCs covered almost the entire inner and outer side of the tubular scaffold and they aligned along their fibrous directions, respectively. The arrangements of ECs and SMCs were consistent with their arrangements in native blood vessels. To further verify the performance of the scaffold in a longer culture period, the scaffold was stained with H&E after one month of culture (Fig. 5b). H&E staining demonstrated that ECs and SMCs grew along the inner and outer walls of the scaffold, respectively, thus eventually forming closed circular cell layers.

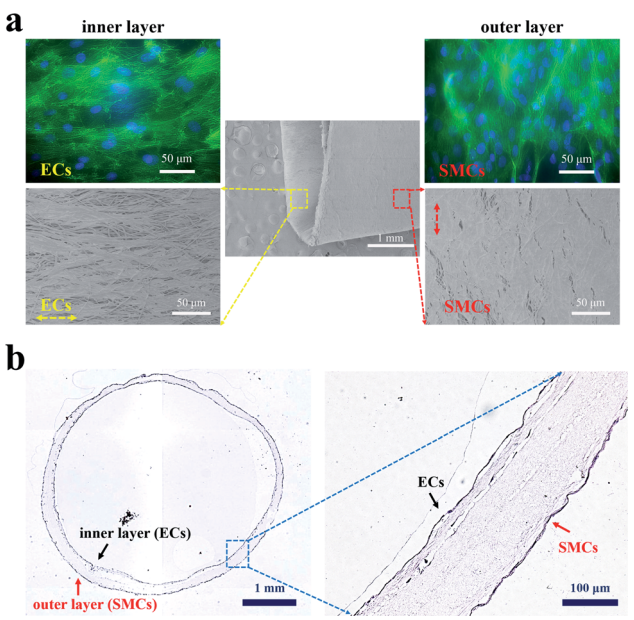

Fig. 5 (a) Fluorescent staining images and SEM images of ECs on the inner layer and SMCs on the outer layer of the PCL tubular scaffold after 10 days of co-culture. The F-actin filaments and nucleus of ECs and SMCs were stained with phalloidin and DAPI solution, respectively. (b) Histological cross-section of the tubular scaffold seeded with ECs and SMCs stained with H&E after one month of co-culture.

3.5. Interactions between ECs and SMCs under the co-culture system

The interactions between ECs and SMCs are essential to the homeostasis of blood vessels.[40] Findings from *in vitro* co-culture models revealed that SMCs could promote the adhesive expression and angiogenesis activity of ECs,[41] and the growth factors released by ECs could also regulate SMC proliferation.[42] This study demonstrated that the double-layer orthogonal tubular scaffold promoted the interaction between ECs and the preservation of the normal contractile phenotype of SMCs.

We first characterized the CD31 expression of ECs cultured for 7 days on the tubular scaffold under individual and co-culture systems. The fluorescence staining images are shown in Fig. 6a and the integrated density histogram is shown in Fig. 6b. The fluorescence intensity in the individual culture group [$(1.25 \pm 0.11) \times 10^6$] was approximately 60% of that in the co-culture group [$(2.17 \pm 0.16) \times 10^6$]. CD31, also known as platelet endothelial cell adhesion molecule 1 (PECAM-1), is mainly expressed at intercellular junctions, especially in regions with endothelial cell–cell adhesion.[43] The enhancement of EC adhesion favours the formation of an endothelial layer. As

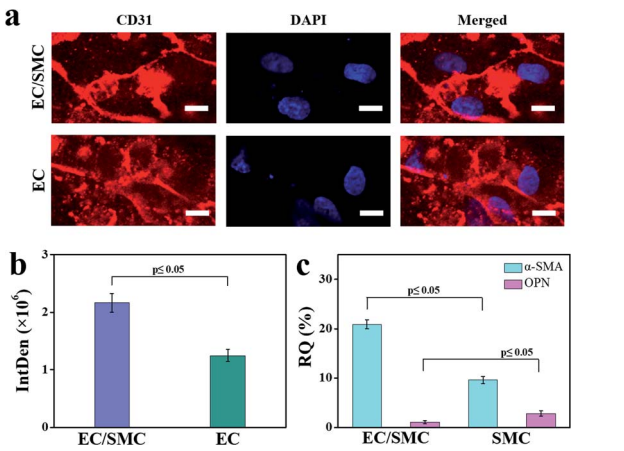

Fig. 6 (a) Fluorescence staining images and (b) quantified fluorescence intensity of CD31 in ECs on the EC/SMC co-culture scaffold and ECs-only culture scaffold. Scale bars are 10 μm. The CD31 and nucleus of ECs and SMCs were stained with mouse anti-CD31 antibody and DAPI solution, respectively. (c) Real-time PCR histogram of α-SMA and OPN of SMCs on the EC/SMC co-culture scaffold (α-SMA: 20.92 ± 0.91%; OPN: 1.09 ± 0.29%) and SMCs-only culture scaffold (α-SMA: 9.61 ± 0.73%; OPN: 2.86 ± 0.51%). The data are presented as mean ± standard error of the mean. Student's two-tailed *t*-test was performed to calculate *p*. Samples were deemed significantly different at a *p*-value < 0.05 ($n = 3$).

a physical barrier, an intact ECs layer forms the structural interface between the circulating blood and the vascular wall, which is essential for maintaining the stability of the vessel and preventing thrombosis. CD31 protein expression in the co-culture system was approximately 1.7-fold higher than that in the EC-only culture system, indicating that co-culture of ECs with SMCs could enhance the adhesion between ECs. SMCs can express and secrete vascular endothelial growth factor (VEGF),[44] which is a mitogen specific to ECs.[33] VEGF can bind to VEGF receptors on the surface of ECs to promote the adhesion between ECs.[45,46] SMCs promote the adhesion between ECs, which may explain why the expression of CD31 in the co-culture system was higher than that in the EC-only culture system.

Next, we measured the mRNA expression levels of α-smooth muscle actin (α-SMA) and osteopontin (OPN) in SMCs that cultured for 1 month in the SMC-only culture and co-culture scaffolds, respectively. α-SMA and OPN are the main genes responsible for the contractile and synthetic phenotypes of SMCs, respectively. Normally, the healthy tunica media of blood vessels exhibits a higher α-SMA expression.[16] The quantitative analyses of α-SMA and OPN expression (Fig. 6c) indicated that the α-SMA gene was more highly expressed (2.2-fold increase) and the OPN gene was less expressed (two-fifths relative expression) in the EC/SMC co-culture scaffold compared to the SMC-only culture scaffold.

SMCs sustain vascular homeostasis through contraction and relaxation.[47] Maintaining the contraction phenotype of SMCs benefits to alleviate intimal hyperplasia and stabilize blood pressure.[48] ECs might inhibit the phenotypic of SMCs from contractile to synthetic by interfering with transforming growth factor-β_1 (TGF-β_1) from the latent state to the active state.[49] Plasmin is a proteolytic enzyme that converts latent state TGF-β_1 to its active state *in vitro*.[50] Activated TGF-β_1 could promote the proliferation of SMCs and the expression of their synthetic phenotype.[49] Therefore, in the co-culture system, plasminogen activator inhibitor (PAI-1) produced by ECs could indirectly block the activation of TGF-β_1 by inhibiting plasmin.[50]

4. Conclusions

Here, we present a simple and cost-effective method to prepare an orthogonal-bilayer PCL tubular scaffold. The ECs successfully grew in the axial direction and SMCs grew in the circumferential direction on this tubular scaffold, thus mimicking the structure of native blood vessels. The orthogonal fibers created a suitable topography that induced the ECs and SMCs to grow in the desired orientations. The prepared tubular scaffold is a co-culture platform that provided relatively independent culture environments for both ECs and SMCs. The expression levels of CD31 and α-SMA in the co-culture scaffolds were approximately 1.7- and 2.2-fold higher than those in the individual culture scaffolds, whereas OPN expression was less than two-fifths compared to the individual cultures. Therefore, the proposed tubular structure enhanced the adhesion between ECs and the contraction phenotype of SMCs, which could promote the stability of blood vessels. Additionally, ECs and SMCs could form closed-cell layers within one month of culture. Taken together, the results presented herein provide important insights into the design of vascular grafts.

Conflicts of interest

There are no conflicts to declare.

Acknowledgements

This work is financially supported by the National Natural Science Foundation of China (No. 31770107 and 21874116).

References

1 E. J. Benjamin, P. Muntner, A. Alonso, M. S. Bittencourt, C. W. Callaway, A. P. Carson, A. M. Chamberlain, A. R. Chang, S. Cheng, S. R. Das, F. N. Delling, L. Djousse, M. S. V. Elkind, J. F. Ferguson, M. Fornage, L. C. Jordan, S. S. Khan, B. M. Kissela, K. L. Knutson, T. W. Kwan, D. T. Lackland, T. T. Lewis, J. H. Lichtman, C. T. Longenecker, M. S. Loop, P. L. Lutsey, S. S. Martin, K. Matsushita, A. E. Moran, M. E. Mussolino, M. O'Flaherty, A. Pandey, A. M. Perak, W. D. Rosamond, G. A. Roth, U. K. A. Sampson, G. M. Satou, E. B. Schroeder, S. H. Shah, N. L. Spartano, A. Stokes, D. L. Tirschwell, C. W. Tsao, M. P. Turakhia, L. B. Van Wagner, J. T. Wilkins, S. S. Wong, S. S. Virani and American Heart Association Council on C. Prevention Statistics and S. Stroke Statistics, *Circulation*, 2019, **139**, e56–e528.
2 H. Qiu, Q. Tu, P. Gao, X. Li, M. F. Maitz, K. Xiong, N. Huang and Z. Yang, *Biomaterials*, 2021, **269**, 120626.
3 Y. Liu, J. Lu, H. Li, J. Wei and X. Li, *Acta Biomater.*, 2015, **11**, 114–125.
4 A. Goins, A. R. Webb and J. B. Allen, *Mater. Sci. Eng., C*, 2019, **97**, 896–912.
5 D. G. Seifu, A. Purnama, K. Mequanint and D. Mantovani, *Nat. Rev. Cardiol.*, 2013, **10**, 410–421.
6 M. A. Redd, N. Zeinstra, W. Qin, W. Wei, A. Martinson, Y. Wang, R. K. Wang, C. E. Murry and Y. Zheng, *Nat. Commun.*, 2019, **10**, 584.
7 S. Pashneh-Tala, S. MacNeil and F. Claeyssens, *Tissue Eng., Part B*, 2016, **22**, 68–100.
8 K. Liu, N. Wang, W. Wang, L. Shi, H. Li, F. Guo, L. Zhang, L. Kong, S. Wang and Y. Zhao, *J. Mater. Chem. B*, 2017, **5**, 3758–3764.
9 J. Schoneberg, F. De Lorenzi, B. Theek, A. Blaeser, D. Rommel, A. J. C. Kuehne, F. Kiessling and H. Fischer, *Sci. Rep.*, 2018, **8**, 10430.
10 J. M. Silva, C. A. Custódio, R. L. Reis and J. F. Mano, *ACS Biomater. Sci. Eng.*, 2016, **2**, 2304–2314.
11 J. S. Choi and T. S. Seo, *Biomicrofluidics*, 2019, **13**, 014115.
12 E. Bosch Rue, L. M. Delgado, F. J. Gil and R. A. Perez, *Biofabrication*, 2020, **13**, 015003.
13 C. Hu, S. Jonchhe, P. Pokhrel, D. Karna and H. Mao, *Chem. Sci.*, 2021, **12**, 10159–10164.
14 D. S. Hariprasad and T. W. Secomb, *Phys. Rev. E: Stat., Nonlinear, Soft Matter Phys.*, 2014, **90**, 053014.

15 C. Yu, M. Xing, L. Wang and G. Guan, *Biomed. Mater.*, 2020, **15**, 035005.
16 Y. Wang, H. Shi, J. Qiao, Y. Tian, M. Wu, W. Zhang, Y. Lin, Z. Niu and Y. Huang, *ACS Appl. Mater. Interfaces*, 2014, **6**, 2958–2962.
17 T. Dvir, B. P. Timko, D. S. Kohane and R. Langer, *Nat. Nanotechnol.*, 2011, **6**, 13–22.
18 B. Sun, X.-J. Jiang, S. Zhang, J.-C. Zhang, Y.-F. Li, Q.-Z. You and Y.-Z. Long, *J. Mater. Chem. B*, 2015, **3**, 5389–5410.
19 T. D. Stocco, N. J. Bassous, S. Zhao, A. E. C. Granato, T. J. Webster and A. O. Lobo, *Nanoscale*, 2018, **10**, 12228–12255.
20 I. Solaberrieta, A. Jimenez, I. Cacciotti and M. C. Garrigos, *Polymers*, 2020, **12**, 1323.
21 K. F. Schuttler, M. W. Bauhofer, V. Ketter, K. Giese, D. A. Eschbach, M. Yenigun, S. Fuchs-Winkelmann and J. R. J. Paletta, *Sci. Rep.*, 2020, **10**, 9557.
22 I. Cacciotti, M. Ciocci, E. Di Giovanni, F. Nanni and S. Melino, *Int. J. Mol. Sci.*, 2018, **19**, 2368.
23 M. Kobayashi, N. Y. Lei, Q. Wang, B. M. Wu and J. C. Dunn, *Biomaterials*, 2015, **61**, 75–84.
24 B. M. Baker and R. L. Mauck, *Biomaterials*, 2007, **28**, 1967–1977.
25 S. Cheng, Y. Jin, N. Wang, F. Cao, W. Zhang, W. Bai, W. Zheng and X. Jiang, *Adv. Mater.*, 2017, **29**, 201700171.
26 A. Bianco, E. Di Federico and I. Cacciotti, *Polym. Adv. Technol.*, 2011, **22**, 1832–1841.
27 M. Rabionet, M. Yeste, T. Puig and J. Ciurana, *Polymers*, 2017, **9**, 328.
28 C. Li, J. Mao, Q. Li, F. Wang, Y. Jiao, Z. Zhang, R. Guidoin and L. Wang, *Biomed. Mater.*, 2019, **14**, 065012.
29 M. Sun, J. Deng and C. Gao, *J. Colloid Interface Sci.*, 2015, **448**, 231–237.
30 S. Mao, Q. Zhang, H. Li, Q. Huang, M. Khan, K. Uchiyama and J. M. Lin, *Anal. Chem.*, 2018, **90**, 9637–9643.
31 D. Rajendran, A. Hussain, D. Yip, A. Parekh, A. Shrirao and C. H. Cho, *J. Biomed. Mater. Res., Part A*, 2017, **105**, 2119–2128.
32 L. Liverani, M. S. Killian and A. R. Boccaccini, *Front. Bioeng. Biotechnol.*, 2019, **7**, 68.
33 G. Neufeld, T. Cohen, S. Gengrinovitch and Z. Poltorak, *FASEB J.*, 1999, **13**, 9–22.
34 A. S. Luyt and S. Gasmi, *J. Mater. Sci.*, 2016, **51**, 4670–4681.
35 S. Singh, B. M. Wu and J. C. Dunn, *Biomaterials*, 2011, **32**, 2059–2069.
36 Y. F. Hsieh, K. Sahagian, F. Huang, K. Xu, S. Patel and S. Li, *Biomed. Mater.*, 2017, **12**, 065004.
37 Q. Li, L. Mu, F. Zhang, Z. Mo, C. Jin and W. Qi, *Mater. Sci. Eng., C*, 2017, **78**, 854–861.
38 X. Jin, X. Geng, L. Jia, Z. Xu, L. Ye, Y. Gu, A. Y. Zhang and Z. G. Feng, *Macromol. Biosci.*, 2019, **19**, e1900114.
39 J. Shi, S. Chen, L. Wang, X. Zhang, J. Gao, L. Jiang, D. Tang, L. Zhang, A. Midgley, D. Kong and S. Wang, *J. Biomed. Mater. Res., Part B*, 2019, **107**, 2040–2049.
40 Y. Pan, J. Yang, Y. Wei, H. Wang, R. Jiao, A. Moraga, Z. Zhang, Y. Hu, D. Kong, Q. Xu, L. Zeng and Q. Zhao, *Adv. Sci.*, 2018, **5**, 1800006.
41 A. A. Ucuzian, D. V. Bufalino, Y. Pang and H. P. Greisler, *Microvasc. Res.*, 2013, **90**, 40–47.
42 J. H. Ryu, E. Y. Jeon and S. J. Kim, *J. Vasc. Res.*, 2019, **56**, 129–138.
43 J. R. Privratsky and P. J. Newman, *Cell Tissue Res.*, 2014, **355**, 607–619.
44 M. Takenaka, K. Hirade, K. Tanabe, S. Akamatsu, S. Dohi, H. Matsuno and O. Kozawa, *Biochem. Biophys. Res. Commun.*, 2003, **301**, 198–203.
45 K. Joensuu, I. Paatero, J. J. Alm, K. Elenius, H. T. Aro, T. J. Heino and T. A. Hentunen, *Scand. J. Surg.*, 2011, **100**, 216–222.
46 H. Yamamoto, H. Rundqvist, C. Branco and R. S. Johnson, *Front. Cell Dev. Biol.*, 2016, **4**, 99.
47 K. E. Steucke, P. V. Tracy, E. S. Hald, J. L. Hall and P. W. Alford, *J. Biomech.*, 2015, **48**, 3044–3051.
48 S. B. H. Timraz, I. A. H. Farhat, G. Alhussein, N. Christoforou and J. C. M. Teo, *Exp. Cell Res.*, 2016, **343**, 168–176.
49 S. Huang, P. Chen, X. Shui, Y. He, H. Wang, J. Zheng, L. Zhang, J. Li, Y. Xue, C. Chen and W. Lei, *J. Pharm. Pharmacol.*, 2014, **66**, 1469–1477.
50 G. B. Nackman, F. R. Bech, M. F. Fillinger, R. J. Wagner and J. L. Cronenwett, *Surgery*, 1996, **120**, 418–426.